Chapter 6
Physics of Wind Parks

Wind parks need special treatment, because here the flow conditions approaching most of the turbines in the park interior are no longer undisturbed. Wakes produced by upwind turbines can massively influence downwind turbines. This includes reduced wind speeds and enhanced levels of turbulence which will lead to reduced yields and enhanced loads. For a given land or sea area, it is desirable to place the wind turbines as close together as possible to maximize energy production. However, if wind turbines are too closely spaced, wake interference effects could result in a considerable reduction in the efficiency of the wind park's energy production. Some wind parks with tightly spaced turbines have produced substantially less energy than expected based on wind resource assessments. In some densely packed parks where turbines have failed prematurely, it has been suspected that these failures might have been caused by excessive turbulence associated with wake effects (Elliot 1991).

A special spatial arrangement of the turbines in smaller wind parks with regard to the mean wind direction may help to minimize wake-turbine interactions. But for larger wind parks, wake-turbine interactions are unavoidable in the park interior and the ratio between mean turbine distance and rotor diameter becomes the main parameter that governs the park efficiency. Before we consider such large wind parks in Sect. 6.2, we will shortly describe the characteristics of single turbine wakes.

6.1 Turbine Wakes

We distinguish between near wake and far wake when looking at turbine wakes. The near wake is taken as the area just behind the rotor, where the special properties of the rotor itself can still be discriminated, so approximately up to a few rotor diameters downstream. We find features such as 3D vortices and tip vortices from single blades in the near wake. The presence of the rotor is apparent by the

S. Emeis, *Wind Energy Meteorology*, Green Energy and Technology,
DOI: 10.1007/978-3-642-30523-8_6, © Springer-Verlag Berlin Heidelberg 2013

number of blades, and blade aerodynamics. The far wake is the region beyond the near wake, where modelling the actual rotor is less important (Vermeer et al 2003).

The wake velocity deficit, the downwind decay rate of the wake, and the added turbulence intensity within the far wake with respect to downwind distance behind wind turbines are largely determined by two factors: the turbine's thrust coefficient [see Eq. (6.13) and Fig. 6.2] and the ambient atmospheric turbulence [often characterized by the parameter 'turbulence intensity', see Eq. (3.10)]. The initial velocity deficit depends on the amount of momentum extracted by the turbine from the ambient flow. Thus, this deficit is a function of the turbine's thrust coefficient. Turbine thrust coefficients are generally highest at low wind speeds around the cut-in wind speed and decrease with increasing wind speed. They approach to very low values above the rated wind speed of the turbine. Nevertheless, published data on wake deficits have often been analyzed as a function of wind speed rather than thrust coefficient. Wake measurement data generally verify that deficits are highest at low wind speeds and lowest at high wind speeds (Elliot 1991). Vermeer et al (2003) give the following relation for the distance-dependent relative velocity deficit in the far wake:

$$\frac{\Delta u}{u_h} = \frac{u_{h0} - u_h}{u_h} = A\left(\frac{D}{s}\right)^n \tag{6.1}$$

where u_h is the wind speed at hub height, D is the rotor diameter, s is the distance from the turbine, and A and n are constants. A depends on the turbine thrust coefficient and increases with it. A varies between 1 and 3 while n takes values between 0.75 and 1.25 and principally depends on the ambient turbulence intensity. The WAsP model (Troen and Petersen 1989) uses a similar approach (Barthelmie and Jensen 2010):

$$\frac{u_h}{u_{h0}} = \left(1 - \sqrt{1 - C_t}\right)\left(\frac{D}{D + ks}\right)^2 \tag{6.2}$$

with the turbine thrust coefficient C_t (see (6.13) and Fig. 6.2) and the wake decay coefficient k. $k = 0.04$ is typical for offshore conditions (Barthelmie and Jensen 2010) while 0.075 is the default value in WAsP (Barthelmie et al (2004).

The added turbulence intensity in the wake decreases more slowly than the velocity deficit. Vermeer et al (2003) give three empirical formulae from three different sources which describe the measured data quite well. According to Quarton (1989) the added turbulence intensity decreases as:

$$\Delta I = \sqrt{I^2 - I_\infty^2} = 4.8 C_T^{0.7} I_\infty^{0.68} \left(\frac{s_N}{s}\right)^{0.57} \tag{6.3}$$

where I_∞ is the undisturbed turbulence intensity, C_T is the thrust coefficient, and s_N is the length of the near wake which is between one and three rotor diameters. The width of the wake is proportional to the one third power of the rotor diameter (see Frandsen et al 2006 for more details):

$$D_W(x) \propto s^{1/3} \tag{6.4}$$

This spreading of the wake with distance downstream of the turbine leads unavoidably to complex wake–wake interactions in larger wind parks. The formulation for multiple wakes in WAsP is a quadratic superposition of the single wakes (bottom-up approach, Barthelmie and Jensen 2010)

$$\left(1 - \frac{u_h}{u_{h0}}\right)^2 = \sum_n \left(1 - \frac{u_{hn}}{u_{h0}}\right)^2 \tag{6.5}$$

with $n = 1,\ldots N$ the contributions from N single wakes. Jensen (1983) derived for an infinite number of turbines in a row the following asymptotic expression:

$$\frac{u_h}{u_{h0}} = 1 - \left(\frac{a}{1-a}\right)\frac{f}{1-f}; \quad f = (1-a)\left(\frac{D}{D+ks}\right)^2 \tag{6.6}$$

with the induction factor $a = 1 - u_h/u_{h0}$ and the mean turbine distance s. Such approaches decisively depend on the geometry of the wind parks and the wind direction relative to the orientation of the turbine rows. We do not want here to deal with the complications for special arrangements of turbines in a wind park, but we want to analyse the overall efficiency of very large wind parks. Therefore, we present an analytical top-down approach in Sect. 6.2 to derive the mean features dominating the efficiency of large wind parks.

Elliot and Barnard (1990), e.g., collected wind data at nine meteorological towers at the Goodnoe Hills MOD-2 wind turbine site to characterize the wind flow over the site both in the absence and presence of wind turbine wakes. The wind turbine wake characteristics analyzed included the average velocity deficits, wake turbulence, wake width, wake trajectory, vertical profile of the wake, and the stratification of wake properties as a function of the ambient wind speed and turbulence intensity. The wind turbine rotor disk at that site spanned a height of 15–107 m. The nine towers' data permitted a detailed analysis of the wake behaviour at a height of 32 m at various downwind distances from 2 to 10 rotor diameters (D). The relationship between velocity deficit and downwind distance was surprisingly linear [i.e. $n = 1$ in (6.1)], with average maximum deficits ranging from 34 % at 2 D to 7 % at 10 D. Largest deficits were at low wind speeds and low turbulence intensities. Average wake widths were 2.8 D at a downwind distance of 10 D. Implications for turbine spacing are that, for a wind park with a 10-D row separation, park efficiency losses would be significantly greater for a 2-D than a 3-D spacing because of incremental effects caused by overlapping wakes. Other interesting wake properties observed were the wake turbulence (which was greatest along the flanks of the wake). The vertical variation of deficits (which were greater below hub height than above), and the trajectory of the wake (which was essentially straight).

6.2 Analytical Model for Mean Wind Speed in Wind Parks

In the 1990s reasoning on nearly infinitely large wind parks was a purely academic exercise. Now, with the planning of large offshore wind farms off the coasts of the continents and larger islands such exercises have got much more importance (Barthelmie et al. 2005; Frandsen et al. 2006, 2009). In principle, two different approaches for modelling the effects of large wind parks are possible: a bottom-up approach and a top-down approach. The bottom-up approach is based on a superposition of the different wakes of the turbines in a wind park. It requires a good representation of each single wake (see Sect. 6.1) in a three-dimensional flow model (Lissaman 1979; Jensen 1983) and a wake combination model. Reviews are given in Crespo et al (1999) and Vermeer et al (2003). Numerically, this approach is supported by large-eddy simulations (LES) today (Wussow et al. 2007; Jimenez et al. 2007; Steinfeld et al. 2010; Troldborg et al. 2010).

The top-down approach considers the wind park as a whole as an additional surface roughness, as an additional momentum sink or as a gravity wave generator in association with a temperature inversion aloft at the top of the boundary layer (for the latter idea see Smith 2010), which modifies the mean flow above it (Newman 1977; Bossanyi et al. 1980; Frandsen 1992). Crespo et al. (1999) rates this latter class of models—although they have not been much used so far at that time—as being interesting for the prediction of the overall effects of large wind farms. Many of these models still have analytical solutions which make them attractive, although they necessarily contain considerable simplifications. Nevertheless, they can be used for first order approximations in wind park design. More detailed analyses require the operation of complex three-dimensional numerical flow models on large computers in the bottom-up approach.

Smith (2010) uses an analogy to atmospheric flow over a mountain range in order to derive his considerations. His model includes pressure gradients and gravity wave generation associated with a temperature inversion at the top of the boundary layer and the normal stable tropospheric lapse rate aloft. The pattern of wind disturbance is computed using a Fast Fourier Transform. The slowing of the winds by turbine drag and the resulting loss of wind farm efficiency is controlled by two factors. First is the size of the wind farm in relation to the restoring effect of friction at the top and bottom of the boundary layer. Second is the role of static stability and gravity waves in the atmosphere above the boundary layer. The effect of the pressure perturbation is to decelerate the wind upstream and to prevent further deceleration over the wind farm with a favourable pressure gradient. As a result, the wind speed reduction in Smith's (2010) approach is approximately uniform over the wind farm. In spite of the uniform wind over the farm, the average wind reduction is still very sensitive to the farm aspect ratio. In the special case of weak stability aloft, weak friction and the Froude Number close to unity, the wind speed near the farm can suddenly decrease; a phenomenon that Smith (2010) calls 'choking'. We will not follow this idea here. Rather, a top-down approach based on momentum extraction from the flow will be presented in more detail in this subchapter.

The derivation of the analytical wind park model shown here is an extension of earlier versions of this model documented in Frandsen (1992), Emeis and Frandsen (1993) and Emeis (2010a). The consideration of a simple, analytically solvable momentum balance of large wind parks in this subchapter will show that the design of a wind park and distance among each other has to take into account the properties of the surface on which they are erected and the thermal stability of the atmosphere typical for the chosen site. The momentum balance presented here will indicate that the distance between turbines in an offshore wind park and the distance between entire offshore parks must be considerably larger than for onshore parks. Turbines will be characterized only by their hub height, rotor diameter and thrust coefficient. Near wake properties are disregarded.

Starting point for the analytical wind park model is the overall mass-specific momentum consumption m of the turbines which is proportional to the drag of the turbines c_t and the wind speed u_h at hub height h:

$$m = c_t u_h^2 \tag{6.7}$$

In an indefinitely large wind park, this momentum loss can only be accomplished by a turbulent momentum flux τ from above. Here, u_0 is the undisturbed wind speed above the wind park, K_m is the momentum exchange coefficient and Δz is the height difference between hub height of the turbines and the undisturbed flow above the wind park (see Fig. 6.1):

$$\frac{\tau}{\rho} = K_m \frac{u_0 - u_h}{\Delta z} \tag{6.8}$$

The turbulent exchange coefficient K_m describes the ability of the atmosphere to transfer momentum vertically by turbulent motion. This coefficient describes an atmospheric conductivity giving the mass-specific momentum flux (physical units: m^2/s^2) per vertical momentum gradient (unit: 1/s). Thus K_m has the dimension of a viscosity (unit: m^2/s). Typical values of this viscosity are between 1 and 100 m^2/s. The main task in the formulation of the analytical park model is to describe the exchange coefficient K_m as function of the outer (surface roughness, thermal stratification of the boundary layer) and inner (drag of the turbines, turbulence generation of the turbines) conditions in the wind park. A major variable in this context is turbulence intensity T_i [see (3.10] for a definition) which is directly proportional to K_m. We obtain from the stability-dependent formulation of Monin–Obukhov similarity in the surface layer (see Sect. 3.1.1):

$$K_m = \kappa u_* z \frac{1}{\phi_m} \tag{6.9}$$

with the von Kármán constant $\kappa = 0.4$, the friction velocity u_* [see (A.13) in the Appendix], the height z and the stability function ϕ_m:

$$\frac{1}{x} \quad \text{for} \frac{z}{L_*} < 0$$

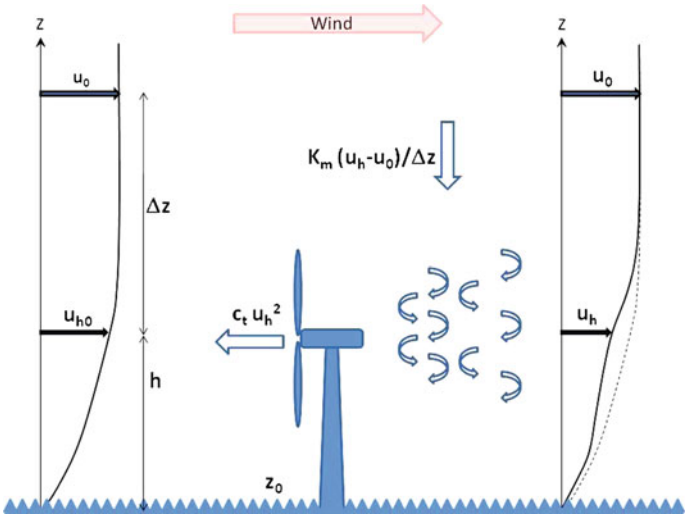

Fig. 6.1 Schematic of momentum loss and replenishment in an indefinitely large wind park. The undisturbed flow is approaching from *left*

$$\phi_m\left(\frac{z}{L_*}\right) = 1 \quad \text{for} \frac{z}{L_*} = 0 \tag{6.10}$$

$$1 + a\frac{z}{L_*} \quad \text{for} \frac{z}{L_*} > 0$$

with $x = (1 - b\ z/L_*)^{1/4}$ and the Obukhov length L_* defined in (3.11). We use $a = 5$ and $b = 16$ in (6.10). Assuming a logarithmic wind profile, the friction velocity, u_* is given by:

$$u_* = u_h \kappa \left(\ln\left(\frac{h}{z_0}\right) - \Psi\left(\frac{\mathrm{h}}{\mathrm{L}_*}\right)\right)^{-1} \tag{6.11}$$

where Ψ is given by (3.15) for unstable conditions and the first equation of (3.21) for neutral and stable conditions.

Following Frandsen (2007), we define the wind park drag coefficient, c_t as a function of the park area A, the rotor area $0.25\pi D^2$, the number of turbines N and the turbine thrust coefficient C_T:

$$c_t = \frac{1}{8}\frac{N\pi D^2}{A} C_T \tag{6.12}$$

C_T is about 0.85 for lower wind speeds around the cut-in wind speed and decreases around and above the rated wind speed of the turbines with increasing wind speed (Barthelmie et al 2006; Jimenez et al 2007). The exact value depends on the construction of the turbine and its operation. We use the following empirical

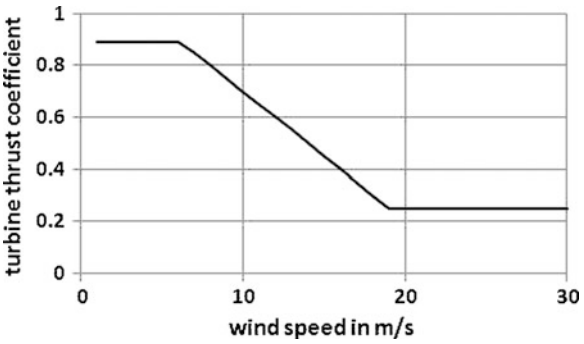

Fig. 6.2 Wind-speed dependent turbine thrust coefficient [see Eq. (6.13)] used in the simple analytical model park model

relation for the thrust coefficient (taken from Fig. 9 in Magnusson 1999) and additionally consider the maximal value at Betz's limit[1]:

$$C_T = \min(\max(0.25; 0.5 + 0.05(14 - u_h)); 0.89) \tag{6.13}$$

Due to (6.13), c_t depends on u_h (see Fig. 6.2) and we have to iterate at least once when we want to solve for u_h later.

The reduction of wind speed in hub height h in the park interior does not only depend on the turbine drag coefficient c_t but also on the roughness of the surface underneath the turbines. This surface roughness can be described by a surface drag coefficient, $c_{s,h}$ observed at height h by rearranging (6.11):

$$c_{s,h} = u_*^2/u_h^2 = \kappa^2 \left(\ln\left(\frac{h}{z_0}\right) - \Psi\left(\frac{\mathrm{h}}{\mathrm{L}_*}\right)\right)^{-2} \tag{6.14}$$

Turbine drag and surface drag can be combined in an effective drag coefficient:

$$c_{teff} = c_t + c_{s,h}. \tag{6.15}$$

There are two ratios describing the wind reduction in the wind park. The reduction of the wind speed at hub height compared to the undisturbed wind speed aloft is denoted by R_u:

$$R_u = \frac{u_h}{u_0} \tag{6.16}$$

The reduction of the wind speed at hub height compared to the undisturbed wind speed upstream of the wind park in the same height h, u_{h0} is denoted by R_t:

[1] The thrust coefficient is the ratio of resistance force T to the dynamic force $0.5\rho u^2{}_0 D$ (rotor area D). The resistance force of an ideal turbine is given by $T = 0.5\rho u^2{}_0 A[4r(1-r)]$ with $r = (u_o - u^*{}_h)/u_0$. $u^*{}_h$ is the mean of u_h and u_0. We have $u^*{}_h = u_0\,(1-r)$. Thus, $C_T = [4r(1-r)]$. For $u_h = 0$ it follows $u^*{}_h = 0.5u_0$, $r = 0.5$ and $C_T = 1$. For $u_h = u_0$ follows $u^*{}_h = u_0$, $r = 0$ and $C_T = 0$. The yield is $P = Tu^*{}_h\, 0.5 = \rho u_0^3 A[4r(1-r)^2]$ and the yield coefficient is $C_P = [4r(1-r)^2]$. For optimal yield at the Betz's limit is r = 1/3 (calculated from $\partial C_P(r)/\partial r = 0$) and $C_T = 8/9$ (Manwell et al. 2009)

$$R_t = \frac{R_u(c_{teff})}{R_u(c_{s,h})} \tag{6.17}$$

using $R_u(c_{s,h}) = u_{h0}/u_0$. Inserting for the exchange coefficient K_m (6.9) and the effective drag coefficient (6.15) in (6.7) yields:

$$c_{teff} u_h^2 = \frac{\kappa u_* z(u_0 - u_h)}{\Delta z \phi_m} \tag{6.18}$$

The height z in (6.18) is essentially $h + \Delta z$, so that the ratio $z/\Delta z$ can be approximated by a constant value:

$$\frac{z}{\Delta z} = f_{h,\Delta z} \tag{6.19}$$

The horizontal turbulence intensity I_u at hub height h is defined by:

$$I_u = \frac{\sigma_u}{u_h} \tag{6.20}$$

The standard deviation of the horizontal wind speed can be parameterized using the friction velocity u_*:

$$\sigma_u = \frac{1}{\kappa} u_* \tag{6.21}$$

which yields the following relation between friction velocity, u_* and turbulence intensity, I_u:

$$u_* = \kappa \sigma_u = \kappa u_h I_u \tag{6.22}$$

Inserting of (6.19) and (6.22) in (6.18) yields finally:

$$c_{teff} u_h^2 = \frac{\kappa^2 u_h (u_0 - u_h)}{\phi_m} f_{h,\Delta z} I_u = \frac{\kappa^2 u_h u_0^2}{u_0 \phi_m} f_{h,\Delta z} I_u - \frac{\kappa^2 u_h^2}{\phi_m} f_{h,\Delta z} I_u \tag{6.23}$$

Rearrangement leads to:

$$c_{teff} u_h^2 + \frac{\kappa^2 u_h^2}{\phi_m} f_{h,\Delta z} I_u = u_h^2 \left(c_{teff} + \frac{\kappa^2}{\phi_m} f_{h,\Delta z} I_u \right) = u_0^2 \frac{R_u \kappa^2}{\phi_m} f_{h,\Delta z} I_u \tag{6.24}$$

and finally to an expression for the ratio (6.16):

$$R_u = \frac{u_h}{u_0} = \frac{u_h^2}{R_u u_0^2} = \frac{\frac{\kappa^2}{\phi_m} f_{h,\Delta z} I_u}{\left(c_{teff} + \frac{\kappa^2}{\phi_m} f_{h,\Delta z} I_u \right)} = \frac{f_{h,\Delta z} I_u}{\left(f_{h,\Delta z} I_u + \frac{\phi_m}{\kappa^2} c_{teff} \right)} \tag{6.25}$$

Thus, the ratio (6.17) between the wind speed at hub height inside the wind park to the undisturbed wind speed upstream is:

$$R_t = \frac{\left(f_{h,\Delta z} I_u + \frac{\phi_m}{\kappa^2} c_{s,h}\right)}{\left(f_{h,\Delta z} I_u + \frac{\phi_m}{\kappa^2} c_{teff}\right)} \tag{6.26}$$

Formulation (6.26) permits easily to add the turbulence intensity produced by the turbines during operation to the upstream turbulence intensity ($I^2_{u,eff} = I^2_{u0} + I^2_{u,t}$). Following Barthelmie et al. (2003) the additional turbulence, $I_{u,t}$ can be parameterized as a function of the thrust coefficient (6.13) using a mean turbine distance normalized by the turbine diameter s:

$$I_{u,t} = \sqrt{\frac{1,2C_T}{s^2}} \tag{6.27}$$

The upper frame in Fig. 6.3—in displaying R_t from (6.24)—shows how much the wind speed at hub height will be reduced as a function of the atmospheric instability and the surface roughness. The presented results have been found for turbines with a hub height of 92 m, a rotor diameter of 90 m and a mean distance between two turbines in the park of 10 rotor diameters. It becomes obvious that the reduction is smallest (a few percent) for unstable thermal stratification of the atmospheric boundary layer and high surface roughness. I.e., the reduction is smallest over a rough land surface with trees and other obstacles for cold air flowing over a warm surface (usually during daytime with strong solar insolation). The largest reduction (up to 45 %) occurs for very smooth sea surfaces when warm air flows over cold waters. This may happen most preferably in springtime. The lower frame of Fig. 6.3 translates this wind speed reduction into a reduction of the available wind power by plotting the third power of R_t from (6.26). The strong stability dependence of the reduction of the available power can be confirmed from measurements at the Nysted wind park in Denmark (Barthelmie et al. 2007).

The dependence of wind and available power reduction as function of surface roughness has consequences for offshore wind parks which will become the major facilities for wind power generation in the near future. The lower turbulence production due to the relative smoothness of the sea surface compared to land surfaces hampers the momentum re-supply from the undisturbed flow above. In order to limit the wind speed reduction at hub height in the interior of the wind park to values known from onshore parks, the turbines within an offshore wind park must have a larger spacing than within an onshore park. Roughly speaking, the number of turbines per unit area in an offshore park with roughness $z_0 = 0.001$ m must be approximately 40 % lower than in an onshore park with $z_0 = 0.1$ m in order to have the same power yield for a given wind speed and atmospheric stability.

Inversely, Eq. (6.26) may be used to determine the optimal areal density of turbines in a large wind park for given surface roughness and atmospheric stability conditions.

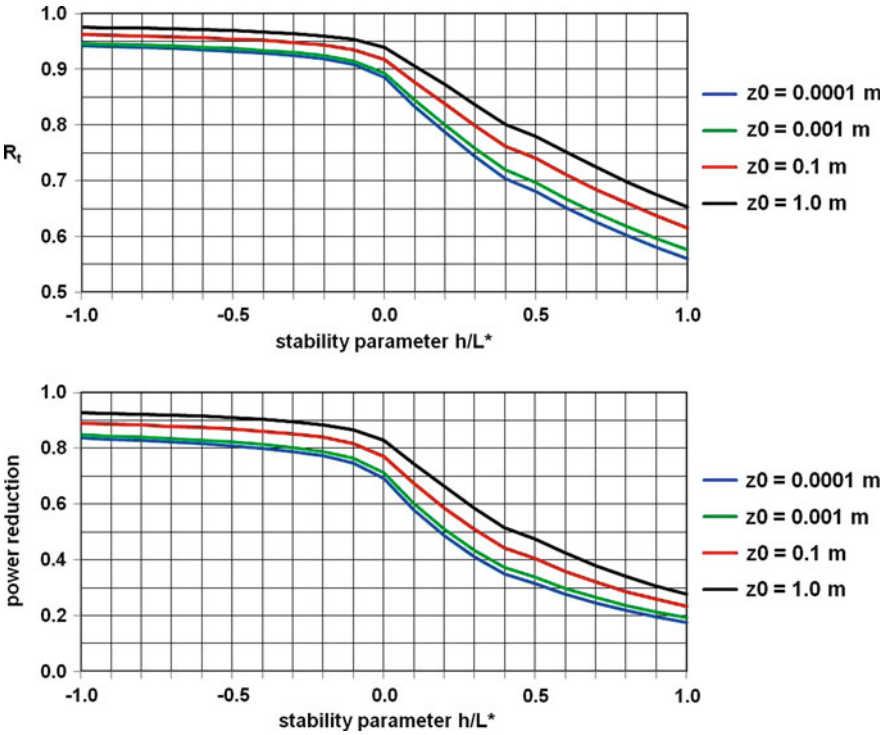

Fig. 6.3 Normalised reduction of wind speed (*above*) and available wind power (*below*) at hub height in an indefinitely large wind park as function of atmospheric instability (h/L* = 1: strong instability, 0: neutral stability, + 1: stable stratification) and surface roughness (z0 = 0.0001 m: very smooth sea surface, 0.001 m: rough sea surface, 0.1 m: smooth land surface, 1.0 m: rough land surface)

6.3 Analytical Model for Wind Park Wakes

The estimation of the length of the wakes of large wind parks is essential for the planning of the necessary distance between adjacent wind parks. This estimation can be made using the same principal idea as in the subchapter before: the missing momentum in the wake of an indefinitely broad wind park can only be replenished from above (Fig. 6.4). If we imagine to move with an air parcel, then we feel the acceleration of the speed of this parcel, u_{hn} from u_{hn0} at the rear end of the park to the original undisturbed value, u_{h0}, which had prevailed upstream of the park (neglecting the Coriolis force):

$$\frac{\partial u_{hn}}{\partial t} = \frac{\partial(\tau/\rho)}{\partial z} \tag{6.28}$$

Substituting the differentials by finite differences and using (6.8) leads to:

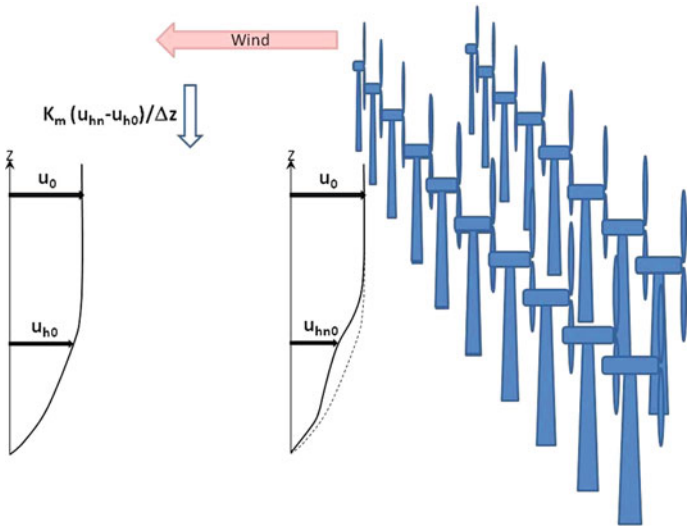

Fig. 6.4 Wind speed u_{hn} (from u_{hno} at the rear end of the wind park to the original undisturbed wind speed further down to the *left* u_{h0}) in the wake of an indefinitely broad wind park

$$\frac{\Delta u_{hn}}{\Delta t} = \frac{\kappa u_* z}{\Delta z^2}(u_{h0} - u_{hn}) = \frac{\kappa u_* z u_{h0}}{\Delta z^2} - \frac{\kappa u_* z u_{hn}}{\Delta z^2} \tag{6.29}$$

This is a first order difference equation of the form:

$$\frac{\Delta u_{hn}}{\Delta t} + \alpha u_{hn} = \alpha u_{h0} \tag{6.30}$$

with $\alpha = \kappa u_* z/\Delta z^2$ and the time-dependent solution:

$$u_{hn}(t) = u_{h0} + C\exp(-\alpha(t - t_0)) \tag{6.31}$$

The constant of integration C can be determined from the initial condition:

$$u_{hn}(t = t_0) = u_{hn0} = u_{h0} + C \tag{6.32}$$

Please note the difference between the undisturbed wind speed u_{h0} at hub height and the wind speed at hub height directly behind the wind park u_{hn0}. Inserting (6.32) in (6.31) yields:

$$u_{hn}(t) = u_{h0} + (u_{hn0} - u_{h0})\exp(-\alpha t) \tag{6.33}$$

Dividing by u_{h0} gives the ratio R_n between the wind speed at hub height in the wake to the undisturbed wind speed in the same height u_{h0}:

$$R_n = \frac{u_{hn}(t)}{u_{h0}} = 1 + \left(\frac{u_{hn0}}{u_{h0}} - 1\right)\exp(-\alpha t) \tag{6.34}$$

The factor α in (6.30), (6.33) and (6.34) depends on the surface roughness and the thermal stratification of the boundary layer via (6.11). This solution is in the time domain. It can be converted into the space domain by assuming an average wind speed over the wake.

The upper frame in Fig. 6.5 shows wake lengths as function of surface roughness for neutral stability ($h/L^* = 0$) by plotting the third power of R_n from (6.34). If we define the distance necessary for a recovery of the available power to 95 % of its undisturbed value upstream of the park as wake length, then we see a wake length of 4 km for rough land surfaces and a wake length of about 18 km for smooth sea surfaces. Figure 6.5 has been produced for the same park parameters as Fig. 6.3. Actually, the results from Fig. 6.3 serve as left boundary conditions for Fig. 6.5. The lower frame of Fig. 6.5 demonstrates the strong influence of atmospheric stability on the wake length for an offshore wind park over a smooth sea surface ($z_0 = 0.0001$ m). Taking once again the 95 % criterion, the wake length for very unstable atmospheric conditions is still about 10 km. For very stable conditions, the wake length is even longer than 30 km. Such long wakes have been confirmed from satellite observations (Christiansen and Hasager 2005).

6.4 Application of the Analytical Model with FINO1 Stability Data

The application of the above analytical model to a real wind park needs the knowledge of the frequency distribution of atmospheric stabilities at the site of the wind park. We give here an example by using the distribution measured at 80 m height at the mast FINO1 in the German Bight for the years 2005 and 2006. Figure 6.6 shows this distribution for the range $-2 \leq z/L_* \leq 2$. 91.16 % of all data fall into this range. The highest frequency occurs for the bin $-0.15 \leq z/L_* \leq -0.05$. The median of the full distribution is at $z/L_* = -0.11$, the median of the range shown in Fig. 6.6 is $z/L_* = -0.07$. Now the above equations for the reduction of wind speed in the park interior (6.26) and the wake length (6.34) are solved for all 41 bins shown in Fig. 6.6 and the resulting values for R_t and R_n are multiplied with the respective frequencies from Fig. 6.6.

Rebinning the resulting R_t and R_n values leads to the distributions shown in Figs. 6.7 and 6.8. The top frame in Fig. 6.7 shows the distribution of wind speed reductions at hub height in the park interior. The most frequent speed reduction R_t is 0.95, the median is 0.93 and the weighted mean is 0.87. The 90th percentile is observed at 0.73 and the 95th percentile at 0.65. The lower frame of Fig. 6.7 gives the resulting reductions in power yield. The most frequent power yield reduction is 0.83, the median is 0.80 and the weighted mean is 0.70. The 90th percentile is observed at 0.37 and the 95th percentile at 0.24.

Figure 6.8 displays the respective distribution of the wake length. Here, the wake length has been defined as above as the distance where the power yields have

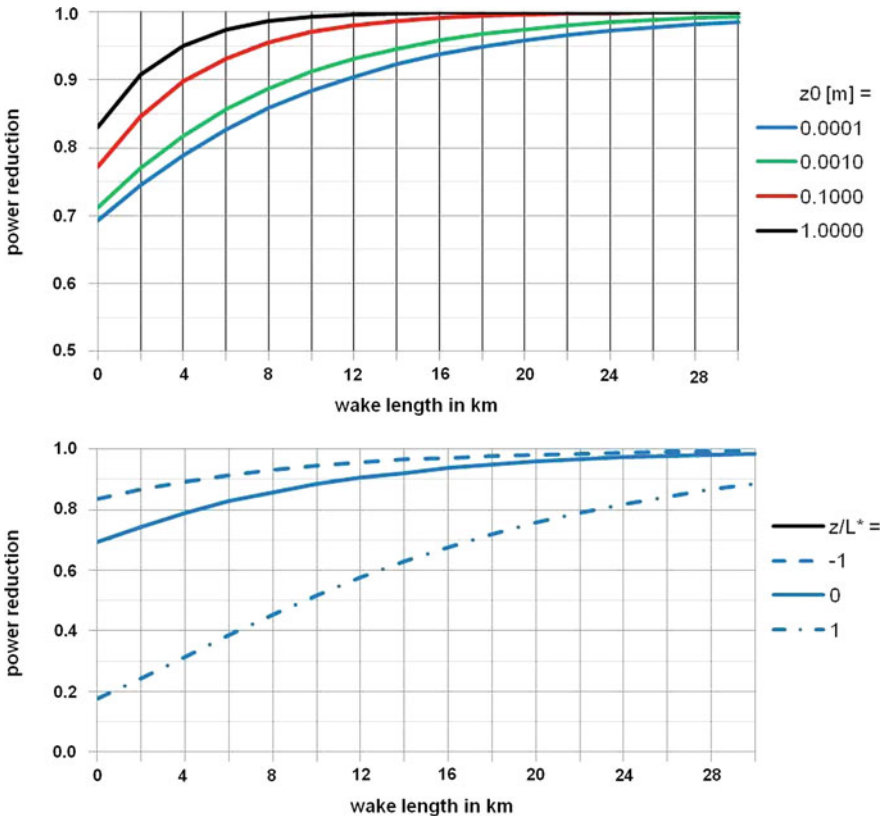

Fig. 6.5 Normalised reduction of available wind power at hub height behind an indefinitely large wind park as function of the distance from the rear side of the park. *Above*: as function of surface roughness (z0 = 0.0001 m: very smooth sea surface, 0.001 m: rough sea surface, 0.1 m: smooth land surface, 1.0 m: rough land surface) with neutral stability. *Below*: as function of atmospheric instability (h/L* = −1: strong instability, 0: neutral stability, + 1: stable stratification) for a smooth sea surface

recovered to 95 % of their original value upstream of the park. The most frequent wake length is 11 km, the median is nearly 14 km and the weighted mean is 17.7 km. The 90th percentile is observed at 31 km and the 95th percentile at 37 km.

6.5 Risks that a Tornado Hits a Wind Park

Tornadoes are a risk for wind turbines. The weakest (F1) tornadoes have a wind speed of 32–50 m/s, while F2 tornadoes reach 70 m/s which is well above the survival speed of wind turbines. But even if the peak wind speed is below the

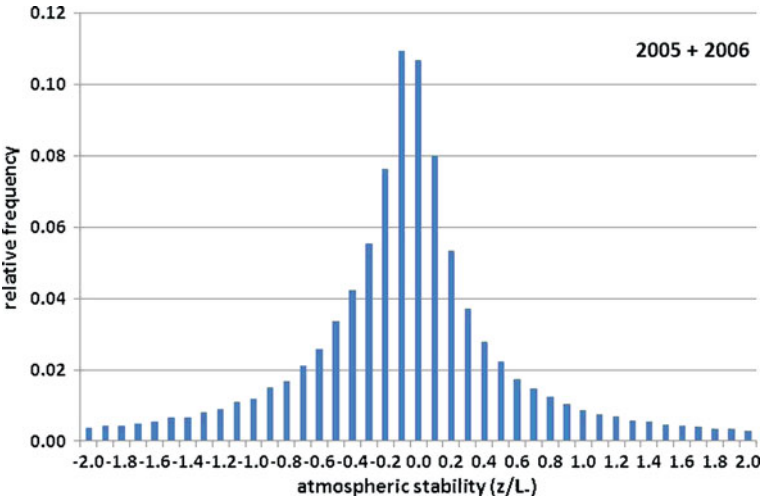

Fig. 6.6 Frequency distribution of atmospheric stability at 80 m height at the mast FINO1 in the German Bight. Bin width is 0.1

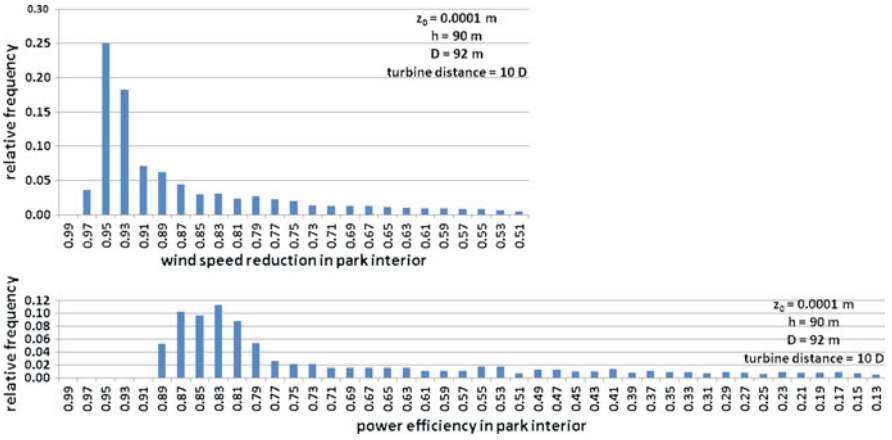

Fig. 6.7 Frequency distribution of wind speed reduction at hub height in the park interior (*top*) and of power yield reduction (*below*) using the stability data from Fig. 6.6. Bin width is 0.02

survival speed, the most dangerous feature is the rapid increase of wind speed connected with a rapid wind direction change when a tornado approaches a wind turbine. There is no reasonable alert time available.

Dotzek et al (2010) investigate the risk that an offshore wind park in the German Bight will be hit by a waterspout. Assuming an area of about 100 km^2 (10 × 10 km^2) as typical for prospective offshore wind parks off the German

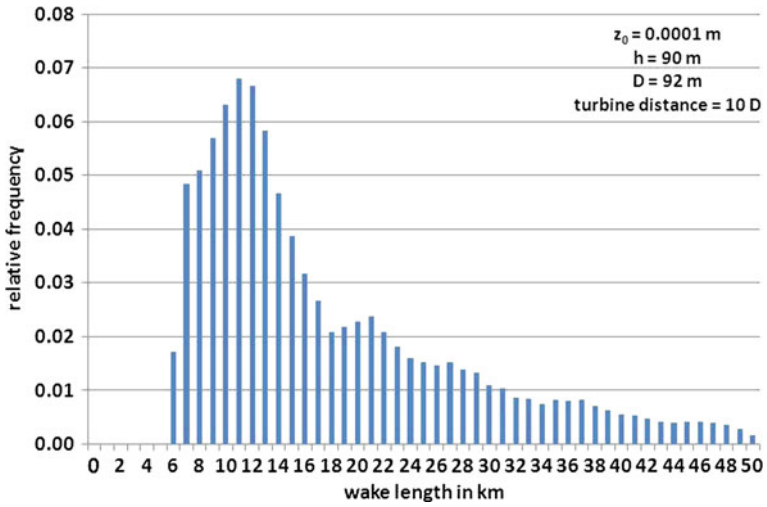

Fig. 6.8 Frequency distribution of the wake length of an indefinitely broad wind park in km using the stability data from Fig. 6.6. Bin width is 1 km. Wake length has been defined as the distance where 95 % of the original power yield is reached again

coast, the probability is estimated that such a wind park will be affected by waterspouts. This estimation does not look for the probability that a single wind turbine is hit by the vortex centre, i.e. the probability of a mathematical point being hit (Thom 1963) is not investigated. Due to the horizontal wind shear across the vortex' core and mantle regions, even a near miss by a waterspout may be hazardous for a wind turbine. In addition, it is presently unclear if the small-scale wind field in a wind park altered by the wind turbine wakes themselves (Christiansen and Hasager 2005) may actually increase the likelihood of a hit once a waterspout enters an array of wind turbines. Therefore, the recurrence time of a waterspout anywhere within the wind park instead of at an individual wind turbine site is analysed.

Taking the waterspout incidence presently known for the German North Sea coast [which is about one tornado per 10,000 km^2 per year, based on estimates by Koschmieder (1946) or Dotzek (2003)], one can expect one tornado in an offshore wind park once within one hundred years. This includes the assumption that waterspouts occur homogeneously over the German Bight area. If using the upper limit of Koschmieder's estimate, which is two waterspouts per 10,000 km^2 per year, this recurrence time reduces to 50 years for a single wind park.

While this still seems to be a long interval, one has to take into account that the total area of approved or actual off-shore wind parks in the German Bight is already 648 km^2 in 2010 (Source: German Federal Maritime and Hydrographic Agency; Bundesamt für Seeschifffahrt und Hydrographie), leading to a recurrence interval of less than eight years for any wind park to be hit by waterspouts in a given year, based on Koschmieder's incidence estimate of two waterspouts per

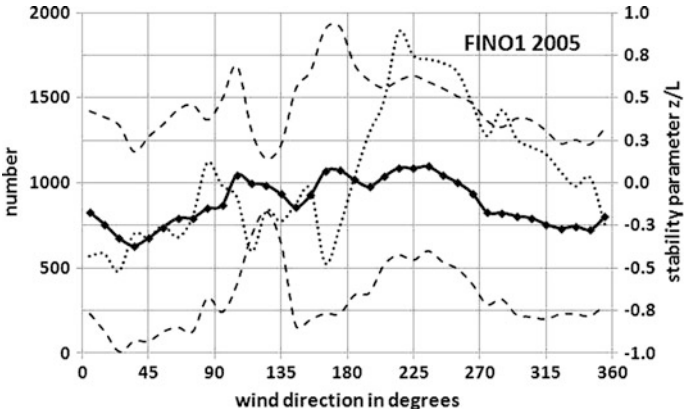

Fig. 6.9 Example for the dependence of the mean stability of the marine boundary layer air for different wind directions from FINO1 data for the year 2005. The full line gives the annual mean stability parameter h/L^* (*right-hand axis*), the dashed lines give the annual mean minus and plus one standard deviation of this stability parameter. The dotted line gives the number of 10 min data per 10 degree wind direction interval (*left-hand axis*)

year per 10,000 km^2. A recent report by the European Wind Energy Association (EWEA 2007) identified that offshore North Sea wind parks with an area of 17,900 km^2 were needed to supply 180 GW, i.e. about 25 % of Europe's current electricity needs. A scenario for 2020 foresees the installation of 40 GW, which would require about 3,980 km^2 of wind parks. Should this scenario materialise, one or more waterspouts within an offshore wind park would have to be expected every other year.

6.6 Summary for Wind Parks

The roughness of the underlying surface on which large wind parks are erected turns out to be a decisive parameter governing the efficiency of such parks. This happens, because the ability of the atmosphere to supply momentum from the undisturbed flow above depends on turbulence intensity, which increases with increasing surface roughness. Therefore, in offshore wind parks, this supply is much less than over land, where turbulence intensity is much higher. Thus, in offshore wind parks, the spacing between the turbines in the park must be larger as onshore. The gaps between adjacent offshore wind parks must be larger as well.

Another important governing parameter for the efficiency of wind parks is the thermal stability of the atmosphere, because turbulence intensity is much higher

for unstable stratification than for stable stratification. Over the ocean stability mainly depends on the type of thermal advection. Cold air advection over warmer water usually leads to unstably stratified boundary layers and warm air advection over cold water to stably stratified boundary layers. In the west wind belts of the temperate latitudes, cold and warm air advection regimes are coupled to different wind directions which correspond to the typical wind directions in the warm and cold sectors of the moving depressions (see Fig. 6.9 for an example). As mean turbine distances and gaps between entire parks can be smaller for unstable stratification than for stable stratification, it might be advisable to make at least the gaps between entire offshore parks wind direction-dependent having larger gaps in the direction of flow that is connected to warm air advection.

The example in Fig. 6.9 shows unstable stratification for north-westerly and northerly winds and stable stratification for south-westerly winds. In such a wind regime, it might be advisable to have larger distances between the turbines and between wind parks in the south-west to north-east direction, while shorter distances are possible in the north-west to south-east direction. The lower frame of Fig. 6.3 shows that there is a factor of two in power reduction between $h/L_* = -0.3$ and $h/L_* = 0.1$, which are the typical mean stabilities in Fig. 6.9. Therefore, the analysis of the relation between average stability of the boundary layer and the wind direction should be analysed during the siting procedure for offshore wind parks. This advice does not apply to onshore wind parks, because here the atmospheric stability mainly depends on cloudiness and time of the day, but not so much on wind direction.

References

Barthelmie, R.J., L. Folkerts, F.T. Ormel, P. Sanderhoff, P.J. Eecen, O. Stobbe, N.M. Nielsen: Offshore Wind Turbine Wakes Measured by Sodar. J. Atmos. Oceanogr. Technol. **20**, 466–477 (2003)

Barthelmie, R., Frandsen, S.T., Rethore, P.E., Jensen, L.: Analysis of atmospheric impacts on the development of wind turbine wakes at the Nysted wind farm. Proc. Eur. Offshore Wind Conf. 2007, Berlin 4.-6.12.2007 (2007)

Barthelmie, R., Hansen O.F., Enevoldsen K., Højstrup J., Frandsen S., Pryor S., Larsen S.E., Motta M., and Sanderhoff P.: Ten Years of Meteorological Measurements for Offshore Wind Farms. J. Sol. Energy Eng. 127, 170–176 (2005)

Barthelmie R.J., L.E. Jensen: Evaluation of wind farm efficiency and wind turbine wakes at the Nysted offshore wind farm. Wind Energy **13**, 573–586 (2010)

Barthelmie, R.J., S. Pryor, S. Frandsen, S. Larsen: Analytical Modelling of Large Wind Farm Clusters. Poster, Proc. EAWE 2004 Delft (2004). (http://www.risoe.dk/vea/storpark/Papers%20and%20posters/delft_013.pdf)

Bossanyi, E.A., Maclean C., Whittle G.E., Dunn P.D., Lipman N.H., Musgrove P.J.: The Efficiency of Wind Turbine Clusters. Proc. Third Intern. Symp. Wind Energy Systems, Lyngby (DK), August 26–29, 1980, 401–416 (1980)

Christiansen, M.B., Hasager, C.B.: Wake effects of large offshore wind farms identified from satellite SAR. Rem. Sens. Environ. 98, 251–268 (2005)
Crespo, A., Hernandez, J., Frandsen, S.: Survey of Modelling Methods for Wind Turbine Wakes and Wind Farms. Wind Energy **2**, 1–24 (1999)
Dotzek, N., S. Emeis, C. Lefebvre, J. Gerpott: Waterspouts over the North and Baltic Seas: Observations and climatology, prediction and reporting. Meteorol. Z. **19**, 115–129 (2010)
Dotzek, N.: An updated estimate of tornado occurrence in Europe. – Atmos. Res. **67–68**, 153–161 (2003)
Elliot, D.L., J.C. Barnard: Observations of Wind Turbine Wakes and Surface Roughness Effects on Wind Flow Variability. Solar Energy, **45**, 265–283(1990)
Elliot, D.L.: Status of wake and array loss research. Report PNL-SA–19978, Pacific Northwest Laboratory, September 1991, 17 pp. (1991) (available from: http://www.osti.gov/energycitations/product.biblio.jsp?osti_id=6211976)
Emeis, S., S. Frandsen: Reduction of Horizontal Wind Speed in a Boundary Layer with Obstacles. Bound.-Lay. Meteorol. **64**, 297–305 (1993)
Emeis, S.: A simple analytical wind park model considering atmospheric stability. Wind Energy **13**, 459–469 (2010a)
EWEA (Eds.): Delivering Offshore Wind Power in Europe. – Report, European Wind Energy Association, Brussels, 32 pp. (2007) [Available at www.ewea.org/fileadmin/ewea_documents/images/publications/offshore_report/ewea-offshore_report.pdf]
Frandsen, S., Jørgensen, H.E., Barthelmie, R., Rathmann, O., Badger, J., Hansen, K., Ott, S., Rethore, P.E., Larsen, S.E., Jensen, L.E.: The making of a second-generation wind farm efficiency model-complex. Wind Energy **12**, 431–444 (2009)
Frandsen, S.: On the Wind Speed Reduction in the Center of Large Cluster of Wind Turbines. J. Wind Eng. Ind. Aerodyn. **39**, 251–265 (1992)
Frandsen, S.: Turbulence and turbulence generated structural loading in wind turbine clusters. Risø-R-1188(EN), 130 pp. (2007)
Frandsen, S.T., Barthelmie, R.J., Pryor, S.C., Rathmann, O., Larsen, S., Højstrup, J., Thøgersen, M.: Analytical modelling of wind speed deficit in large offshore wind farms. Wind Energy **9**, 39–53 (2006)
Jensen, N.O.: A Note on Wind Generator Interaction. Risø-M-2411, Risø Natl. Lab., Roskilde (DK), 16 pp. (1983) (Available from http://www.risoe.dk/rispubl/VEA/veapdf/ris-m-2411.pdf
Jimenez, A., A. Crespo, E. Migoya, J. Garcia: Advances in large-eddy simulation of a wind turbine wake. J. Phys. Conf. Ser., **75**, 012041. DOI: 10.1088/1742-6596/75/1/012041(2007)
Koschmieder, H.: Über Böen und Tromben (On straight-line winds and tornadoes). Die Naturwiss. **34**, 203–211, 235–238 (1946) [In German]
Lissaman, P.B.S.: Energy Effectiveness of arbitrary arrays of wind turbines. AIAA paper 79-0114 (1979)
Magnusson, M.: Near-wake behaviour of wind turbines. J. Wind Eng. Ind. Aerodyn. **80**, 147–167 (1999)
Manwell, J.F., J.G. McGowan, A.L. Rogers: Wind Energy Explained: Theory, Design and Application. 2nd edition. John Wiley & Sons, Chichester. 689 pp. (2010)
Newman, B.G.: The spacing of wind turbines in large arrays. J. Energy Conversion **16**, 169–171 (1977)
Quarton, D.C.: Characterization of wind turbine wake turbulence and its implications on wind farm spacing. Final Report ETSU WN 5096, Department of Energy of the UK. Garrad-Hassan Contract (1989)
Smith, R.B.: Gravity wave effects on wind farm efficiency. Wind Energy, **13**, 449–458 (2010).
Steinfeld, G., Tambke, J., Peinke, J., Heinemann, D.: Application of a large-eddy simulation model to the analysis of flow conditions in offshore wind farms. Geophys. Res. Abstr. **12**, EGU2010-8320 (2010)
Thom, H.C.S.: Tornado probabilities. – Mon. Wea. Rev. **91**, 730–736 (1963)

Troen, I., E.L. Petersen: European Wind Atlas. Risø National Laboratory, Roskilde, Denmark. 656 pp. (1989)

Troldborg, N., J.N. Sørensen, R. Mikkelsen: Numerical simulations of wake characteristics of a wind turbine in uniform inflow. Wind Energy **13**, 86–99 (2010)

Vermeer, L.J., J.N. Sørensen, A. Crespo: Wind turbine wake aerodynamics. Progr. Aerospace Sci. **39**, 467–510 (2003)

Wussow, S., L. Sitzki, T. Hahm: 3D-simulations of the turbulent wake behind a wind turbine. J. Phys. Conf. Ser., **75**, 012033, DOI: 10.1088/1742-6596/75/1/012033 (2007)